Monthly Notices of the ROYAL ASTRONOMICAL SOCIETY
MNRAS **511,** 2349–2355 (2022) https://doi.org/10.1093/mnras/stab3357

ExoMol molecular line lists – XLIII. Rovibronic transitions corresponding to the close-lying X $^2\Pi$ and A $^2\Sigma^+$ states of NaO

G. B. Mitev,[1] S. Taylor,[1] Jonathan Tennyson,[1]★ S. N. Yurchenko,[1] A. A. Buchachenko[2] and A. V. Stolyarov[3]

[1]*Department of Physics and Astronomy, University College London, Gower St, London WC1E 6BT, UK*
[2]*Skolkovo Institute of Science and Technology, Skolkovo Innovation Center, Moscow 121205, Russia*
[3]*Department of Chemistry, Lomonosov Moscow State University, Moscow 119991, Russia*

Accepted 2021 November 15. Received 2021 November 13; in original form 2021 October 15

ABSTRACT

The sodium monoxide radical (NaO) is observed in night-glow in the Earth's mesosphere and likely has astronomical importance. This study concerns the optical transitions within the ground X $^2\Pi$ state and to the very low-lying ($T_e \approx 2000$ cm^{-1}) excited A $^2\Sigma^+$ state. A line list consisting of rovibronic term values, allowed electric dipole transitions, Einstein coefficients, and partition functions for varying temperature are produced using a variational solution of the coupled-channel Schrödinger equations using the program DUO. multi-reference configuration interaction (MRCI) *ab initio* calculations characterizing the potential energy curves of the two states, spin-orbit and *L*-uncoupling non-adiabatic matrix elements, as well as permanent and transition dipole moments were integral in the formation of the final deperturbation model. *Ab initio* potential energy curves are represented in the analytical Extended Morse Oscillator form and refined, along with the spin-orbit and *L*-uncoupling functions, by least-squares fitting to the available spectroscopic data. The input experimental data consisted of pure rotational transitions within the fine-structure components of the X $^2\Pi$ state for $v'' \in [0, 3]$ vibrational levels as well as the rovibronic A $^2\Sigma^+(v' = 0) \leftarrow$ X $^2\Pi(v'' = 0)$ transitions, both with limited coverage over rotational excitation. The lack of data detailing the vibrational structure of the X and A states points to the need for further experimental study of higher excited levels, which would provide a more robust spectroscopic model. The NaO NaOUCMe line list is available via www.exomol.com and the CDS data base.

Key words: molecular data – Earth – planets and satellites: atmospheres.

1 INTRODUCTION

Air-glow, sometimes referred to as night-glow, was first reported by Slipher (1929) and has been identified as the emission of Na D-lines. It has been proposed that these lines arise from the Chapman mechanism (Chapman 1939; Sarkhel et al. 2010; Plane et al. 2012), with some modifications suggested in light of modern measurements (Slanger et al. 2005; Sarkhel et al. 2010), as given by

$$\mathrm{Na} + \mathrm{O_3} \xrightarrow{k_1} \mathrm{NaO} + \mathrm{O_2} \tag{1}$$

$$\mathrm{NaO} + \mathrm{O} \xrightarrow{\alpha k_2} \mathrm{Na}(^2P) + \mathrm{O_2} \tag{2}$$

$$\xrightarrow{(1-\alpha)k_2} \mathrm{Na}(^2S) + \mathrm{O_2} \tag{3}$$

$$\mathrm{Na}(^2P) \rightarrow \mathrm{Na}(^2S) + h\nu(\mathrm{D_1}, \mathrm{D_2}), \tag{4}$$

where $k_{1,2}$ are the temperature-dependent rate constants, α is the branching ratio, and $\mathrm{D}_{1,2}$ are the D-line transition energies.

This mechanism suggests that Na atoms, which are assumed to be ablated from meteors, react with O_3 in the atmosphere to form NaO, which then re-reacts with O atoms to reform Na. Long-lasting visible meteor trails have been attributed to the production of electronically excited Na by the said reaction chain (Kolb & Elgin 1976; Joo et al. 1999). In the Chapman mechanism, the rate-limiting reaction is the formation of NaO, see equation (1). As this reaction takes place in the mesosphere, the variation of mesospheric ozone concentration affects Na air-glow intensity. Because altitude profiles of ozone are available, ozone concentration variation can be used for a deeper study of sodium air-glow and subsequently NaO (Plane 2003; Sarkhel et al. 2010).

Experimental spectroscopic data related to optical transitions of the gas-phase NaO molecules are very sparse. Yamada, Fujitake & Hirota (1989) have provided comprehensive microwave data on the pure rotational transitions of the ground X$^2\Pi$ electronic state for the lowest vibrational $v'' = 0, 1, 2, 3$ levels. However, no experimental data on rovibrational transitions are available, and hence the separations between vibrational levels are not yet experimentally determined. Some information is available on the B $^2\Pi \rightarrow$ X $^2\Pi$ emission spectrum; however, this is unassigned with no characterization of the B state (Pfeifer & Gole 1984; Pugh et al. 1996), which sometimes is assigned as the C $^2\Pi$ state (Langhoff, Partridge & Bauschlicher 1991). The only experimental observation of the lowest excited A $^2\Sigma^+$ state is by Joo et al. (1999), who could assign a handful of the low rotational levels $J = [4.5, 19.5]$ belonging to the rovibronic A $^2\Sigma^+(v' = 0) -$ X $^2\Pi(v'' = 0)$ transitions.

★ E-mail: j.tennyson@ucl.ac.uk

The electronic structure of NaO demonstrates pronounced ionic inter-atomic bonds, leading to large permanent dipoles as well as the close-lying ground X $^2\Pi$ and first excited A $^2\Sigma^+$ state converging to different dissociation thresholds. The low-excitation energy of the A $^2\Sigma^+$ state means that its spin-allowed A–X electronic transition lies in the infrared, largely in the 3- to 5-μm region. From the theoretical viewpoint, the A and X states are expected to be strongly coupled to each other owing to spin-orbit and electronic-rotational intramolecular perturbations. *Ab initio* potential energy curves (PECs) and permanent dipole moments are available for the two lowest electronic states (Buenker & Liebermann 2009; Langhoff et al. 1991; Soldán et al. 1999). However, the corresponding non-adiabatic coupling matrix elements are not known so far.

In this paper we present new *ab initio* PECs for both X $^2\Pi$ and A $^2\Sigma^+$ states of NaO accompanied by spin-orbit and *L*-uncoupling non-adiabatic matrix elements, which we tune to the limited available spectroscopic data. Finally, a rovibronic line list for NaO is simulated to be suitable for modelling spectra up to a temperature of 2500 K. This line list is constructed as part of the ExoMol project (Tennyson & Yurchenko 2012). We note that a previous ExoMol line list for CaO (Yurchenko et al. 2016b), constructed using similar methodology to that employed here, was used by Berezhnoy et al. (2018) to assign a spectrum of CaO in the wake of the Beneshov bolide at a height of 29 km above the Earth's surface.

2 METHOD

2.1 *Ab initio* electronic structure calculation

The initial set of required PECs, and permanent and transition dipole moments for the ground X $^2\Pi$ and near-lying excited A $^2\Sigma^+$ states of NaO were obtained in the framework of *ab initio* electronic structure calculations, which were accompanied by the evaluation of the relevant non-adiabatic matrix elements for the spin-orbit and Coriolis (electron-rotational) coupling. Scalar relativistic effects were introduced by means of the second-order Douglas–Kroll Hamiltonian (Reiher & Wolf 2004). All calculations were performed in the range of internuclear distance $R \in [1.0, 5.0]$ Å using the MOLPRO program suite (Werner et al. 2010).

For both Na and O atoms, aug-cc-pVQZ all electrons basis sets were used. The optimized molecular orbitals (MOs) were generated using the state-averaged self-consistent field (SA-CASSCF) method (Werner & Knowles 1985), taking the lowest doublet (1-3)Π, (1)Σ^+, (1)Σ^-, and (1)Δ states with equal weights. Internally contracted multireference configuration interaction (MR-CISD) calculations (Knowles & Werner 1992) followed, in which the impact of higher excitation on the correlation energy was taken into account implicitly using the Davidson correction (Langhoff & Davidson 1974). For both the SA-CASSCF and MR-CISD steps, the active space consisted of $7a_1$, $3b_1$ and $3b_2$ orbitals corresponding to the point group symmetry C_{2v}, while the lowest two a_1 orbitals were kept doubly occupied. The full counterpoise correction (Boys & Bernardi 1970) was accounted for in each state individually, with the residual size-consistency error eliminated at $R = 20$ Å.

Both permanent and transition dipole moments as well as non-adiabatic *L*-uncoupling matrix elements were computed using the MR-CISD wave functions. The same wave functions and the full Breit–Pauli operator were used to compute the spin-orbit couplings (SOCs) (Berning et al. 2000).

2.2 Fitting procedure

The adiabatic PECs *ab initio* calculated above in Section 2.1 were combined with the relevant SOC and *L*-uncoupling functions in order to evaluate the values of non-adiabatic rovibronic terms and corresponding multichannel wave functions for the mutually perturbed X $^2\Pi$ and A $^2\Sigma^+$ states of NaO. However, the pure *ab initio* estimates are *a priori* and are not accurate enough to predict the rovibronic energy with the spectroscopic accuracy required. For better agreement between predicted and observed transitions, PECs and coupling curves are refined by making constrained adjustments to the parameters that describe them (see below). This is done by a least-squares fitting to experimental data and is performed in DUO, an open-source FORTRAN 2009 program that provides variational solutions to the coupled rovibronic Schrödinger equations for a general open-shell diatomic molecule (Yurchenko et al. 2016a).

The input set of the experimental data taken from Yamada et al. (1989) consisted of pure rotational transition frequencies (with $\Delta v_X = 0$ and $v_X = 0, 1, 2, 3$) up to $J'' = 16.5$. Joo et al. (1999) provided rovibronic frequencies for the A – X (0,0) band up to $J'' = 15.5$, together with relative absorption intensities. Joo *et al.* also observed the $v' - v'' = 1$ band, suggesting an A $^2\Sigma^+$ state vibrational spacing of 498.9 cm^{-1}. This spacing was included in the present fit using an artificial $A(v' = 1) - A(v'' = 0)$ line for $J' = J'' = 0.5$.

The *ab initio* point-wise PECs of both states treated were approximated using the fully analytical Extended Morse Oscillator (EMO) form (Lee et al. 1999; Yurchenko et al. 2016a; Le Roy 2017):

$$V_{\rm EMO}(r) = T_{\rm e} + D_{\rm e}\left[1 - e^{-\beta(r)(r-r_{\rm e})}\right]^2, \tag{5}$$

where $T_{\rm e}$ is the electronic term, $D_{\rm e}$ is the dissociation energy, and $r_{\rm e}$ is the equilibrium distance. In contrast to the conventional Morse potential, the *r*-dependent exponent coefficient $\beta(r)$ in equation (5) is defined as the polynomial series

$$\beta(r) = \sum_{i=0}^{N} \beta_i [y_p(r)]^i; \quad N = \begin{cases} N_+ & \text{for } r > r_{\rm e} \\ N_- & \text{for } r \le r_{\rm e} \end{cases} \tag{6}$$

with respect to the reduced coordinate

$$y_p(r) = \frac{r^p - r_{\rm e}^p}{r^p + r_{\rm e}^p}, \tag{7}$$

which was first introduced by Šurkus, Rakauskas & Bolotin (1984).

In the first step, the EMO potentials (5) were least-squares fitted to the original *ab initio* PECs in PYTHON. The electronic energy of the ground state was fixed to zero, and both PECs were fitted to fourth order in the $\beta(r)$ polynomial expansion (6). The parameter p in equation (7) was fixed to 6 and 4 for the ground and the excited state, respectively.

In the second step, the resulting *ab initio* EMO PECs were refined by adjusting to the experimental transition frequencies (Joo et al. 1999; Yamada et al. 1989), where only β_0(X, A), $T_{\rm e}$(A), $r_{\rm e}$(X) and $r_{\rm e}$(A) fitting parameters were varied. Furthermore, both diagonal, $A_{\rm SO}(r)$, and off-diagonal, $\xi_{\rm AX}(r)$, SOC functions as well as the *L*-uncoupling function, $L_{\rm AX}(r)$, between the A $^2\Sigma^+$ and X $^2\Pi$ states were also fitted simultaneously with the trial EMO PECs above. This was done using the facility in DUO to adjust curves using a *morphing* function, $f_{\rm C}$:

$$f_{\rm C}^{\rm morphed}(r) = f_{\rm C}(r) f_{\rm c}^{ab}(r), \tag{8}$$

where C is the coupling curve in question. $f_{\rm c}^{ab}(r)$ are the original *ab initio* point-wise functions interpolated by ordinary cubic splines with so-called natural boundary conditions. The morphing function, $f_{\rm C}(r)$, in equation (8) is tacitly assumed to be an analytical function of

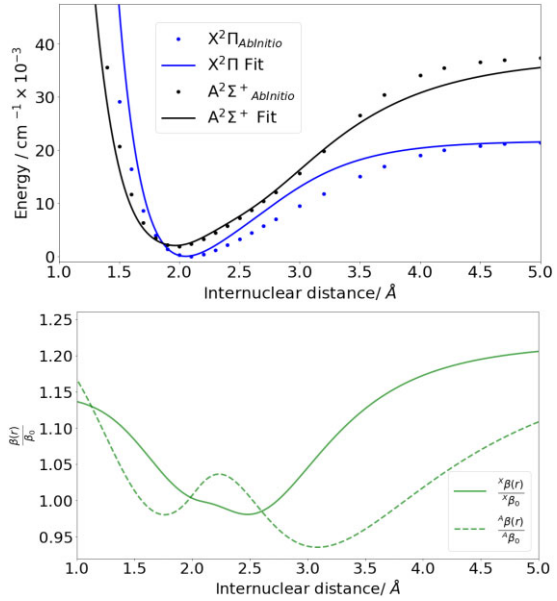

Figure 1. (Top panel) Empirical EMO (fitted) and original *ab initio* point-wise potential energy curves obtained for the X $^2\Pi$ and A $^2\Sigma^+$ states of NaO. (Bottom panel) Distance-dependent exponent coefficient for X $^2\Pi$ and A $^2\Sigma^+$ state EMO fits as normalized by $\beta_0 = A_0$.

Table 1. Root-mean squares errors Δ(rms) in cm^{-1} comparing the fitted model to (a) Yamada et al. (1989) and (b) Joo et al. (1999) rotational transitions.

v_x	Δ_a	Δ_b
0	0.002664	0.022501
1	0.002846	0.679901[a]
2	0.002758	
3	0.017115	
Average	0.006345	0.351201

Note.[a] artificial line, see Section 2.2.

the internuclear distance r, and it was modelled by the linear function

$$f_C(r) = B_0(1 - y_p(r)) + y_p(r)B_\infty \quad (9)$$

of the Šurkus-like variable, $y_p(r)$ (see equation 7), where the equilibrium distance r_e is substituted for the fixed parameter $r_0 = 2.053$ Å . The parameters $p = 6$ and $B_\infty = 1$ are also fixed for all morphing functions, and only the B_0 parameter is kept variable.

Morphing (equation 8) was used, as it avoids the need for an analytical representation of the *ab initio* point-wise coupling curves by changing their original shapes directly. This approach is, however, not normally applied for PECs because of the difficulty in controlling the equilibrium parameter r_e, which is a value of interest not explicitly derivable from this morphing form.

3 RESULTS AND DISCUSSION

3.1 Potential energy curves, spin-orbit and *L*-uncoupling matrix elements

The resulting *ab initio* adiabatic PECs obtained for the X and A states of NaO are depicted in Fig. 1, together with their empirical (adjusted) counterparts. The fitted parameters of the EMO potentials (5) for the two states treated are collected in Table 2. The corresponding *ab initio* diagonal spin-orbit function, $A_{SO}(r)$, of the ground X state as well as the off-diagonal SOC, $\xi_{AX}(r)$, and the L-uncoupling, $L_{AX}(r)$, functions are shown in Fig. 2. The relevant morphing parameters for these functions are given in Table 2.

Table 2. PEC and morphing parameters obtained for the X $^2\Pi$ and A $^2\Sigma^+$ states of NaO. For the definition of the EMO parameters see equation (5), and for morphing parameters see equation (9).

	PEC parametrization	
EMO parameter	X $^2\Pi$	A $^2\Sigma^+$
T_e	0	2029.147[a]
r_e	2.05189[a]	1.96723[a]
D_e	21735.7	35496.4
p	6	4
N_-^b	2	2
N_+^b	4	4
β_0	1.50708327083484[a]	0.989061691136872[a]
β_1	−0.04809897091909	0.181504940347642
β_2	0.16743487156786	0.424100841906937
β_3	−0.95627676523677	−2.926458322108940
β_4	1.16624139895144	2.522897112151440
	B_0^a parameters used for morphed coupling functions[c]	
Function	B_0	
A_{so}	1.0098	
ξ_{AX}	0.6277	
L_{AX}	-0.7455	

Notes.[a] Value achieved via varying in DUO. All others parameters were fixed. [b] As in equation (5), the N_- and N_+ values indicate the limits to which the expansion is summed depending on whether $r < r_e$ or $r > r_e$, respectively. [c] For morphing parameters: as per Section 2.2, $r_0 = 2.053$ Å, $p = 6$, $B_\infty = 1$ (standard when using morphing) for all three f_C.

The fitted EMO PECs and coupling functions reproduce the input experimental data with an overall root-mean-square (rms) error of ∼0.086 cm^{-1}. This rms is deceptively large owing to the pronounced discrepancy of the A $^2\Sigma^+$ artificial line, which skews the mean rms (see Table 1). Indeed, for the ground X $^2\Pi$ state, there is agreement with the experiment on the order of ∼0.006 cm^{-1}, and for the A(v′ = 0) ← X(v″ = 0) case there is agreement on the order of ∼0.02 cm^{-1}.

The *ab initio* $L_{AX}(r)$ function obeys Van Vleck's hypothesis (Mulliken & Christy 1931) of *pure precession* in the interval $r \in [1.3, 3.7]$ Å:

$$L_{AX}(r) \approx \sqrt{L(L+1) - |\Lambda|(|\Lambda| \pm 1)} = \sqrt{2}, \quad (10)$$

where the total electronic angular momentum of molecule L is equal to 1, while its projection on the internuclear axis is zero. Moreover, the relationship

$$\xi_{AX}(r) \approx A_{SO}(r)L_{AX}(r)/2 \approx A_{SO}(r)/\sqrt{2} \quad (11)$$

between diagonal and off-diagonal spin-orbit functions is valid as well.

The *ab initio* SO splitting of the ground X state is found to be close to the empirical A_{SO} value determined by Yamada et al. (1989) (see Table 3). The reliability of the *ab initio* off-diagonal spin-orbit L-uncoupling functions is indirectly confirmed by a good agreement of the Λ-doubling constants (p, q) empirically obtained for the regular perturbed levels of the ground state by Yamada et al. (1989), with their theoretical counterparts roughly estimated for the lowest vibrational levels, v_X, according to the relations (Lefebvre-Brion & Field 2004; Pazyuk, Stolyarov & Pupyshev 1994):

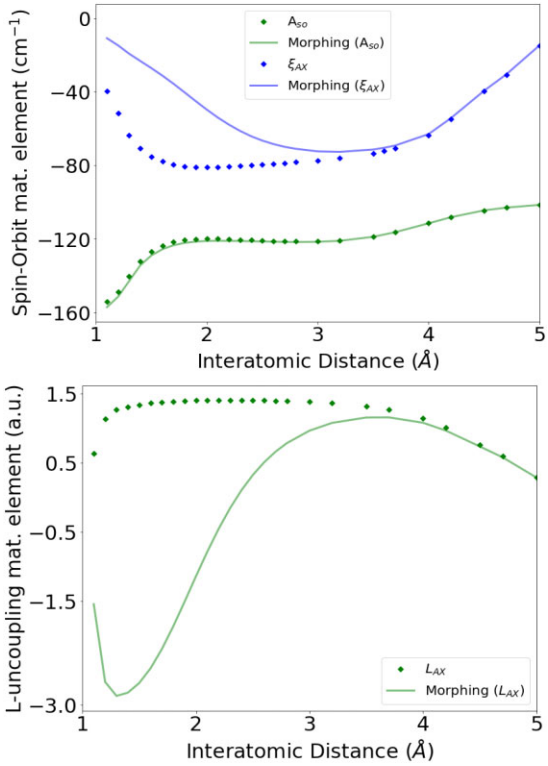

Figure 2. (Top panel) Diagonal, $A_{SO}(r)$, and off-diagonal, $\xi_{AX}(r)$, spin-orbit coupling curves *ab initio* calculated for the X and A states. (Bottom panel) $L_{AX}(r)$ is the corresponding non-adiabatic matrix element of the electron-rotational interaction between the X state and A state.

Table 3. Comparison of *ab initio* calculated spin-orbit splitting (A_{so}) and Λ-doubling constants (p, q) of the ground NaO state with their empirical counterparts taken from Yamada et al. (1989). All values are in cm^{-1}.

Parameter	Empirical	*Ab initio*
A_{so}	−107	−120
p	+ 0.044	+ 0.04
q	+ 0.0003	+ 0.0003

$$p = 2\langle v_X|B\xi_{AX}L_{AX}/\Delta U_{XA}|v_X\rangle \quad (12)$$

$$q = 2\langle v_X|[BL_{AX}]^2/\Delta U_{XA}|v_X\rangle \quad (13)$$

where $B = 1/2\mu R^2$, μ is the reduced molecular mass, $\Delta U_{XA} = U_X - U_A$ is the difference of PECs, while $|v_X\rangle$ are the vibrational wavefunctions of the ground state.

3.2 Permanent and transition dipole moments

The *ab initio* permanent dipole moments $d_{XX}(r)$, $d_{AA}(r)$ calculated for the $X^2\Pi$ and $A^2\Sigma^+$ states of the NaO molecule are given in Fig. 3, together with the corresponding A–X transition dipole moment $d_{AX}(r)$. The present dipole moments are in a good agreement with their previous theoretical counterparts computed by Langhoff et al. (1991).

According to the expected ion-pair character of the interatomic bond, the permanent dipole moments of both A and X states are rapidly increasing linear functions of r, while the corresponding A–X electronic transition dipole moment is very small, but not negligible (see Fig. 3). The maximal values of the present A–X transition

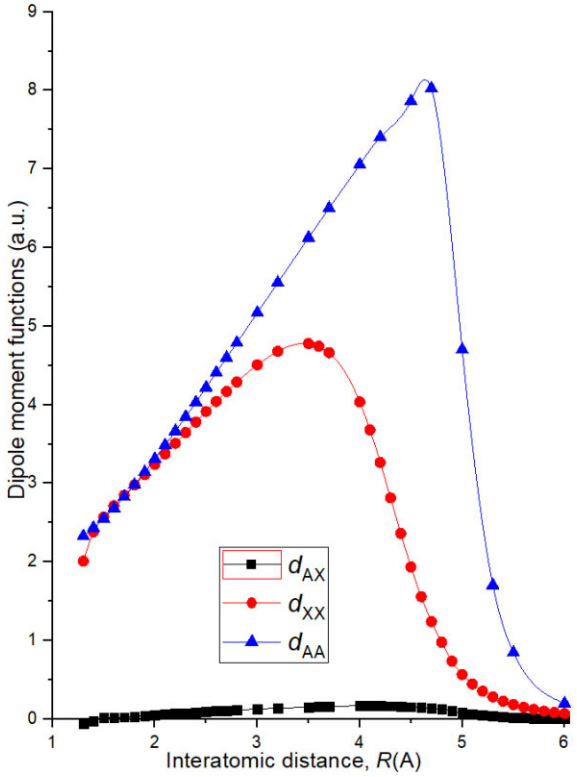

Figure 3. Permanent, $d_{XX}(r)$, $d_{AA}(r)$, and transition, $d_{AX}(r)$, *ab initio* dipole moment functions calculated for the X and A states of the NaO molecule.

moment are about 0.1–0.15 a.u., which agree well with the estimate $|d_{AX}| < 0.2$ D given in Joo et al. (1999). At $r > 3.5$ Å, the ground-state permanent dipole decreases owing to the avoided crossing effect with the excited $C\,^2\Pi$ state. An even more abrupt drop in the permanent dipole is observed for the A state but at larger internuclear distances, presumably also as a result of an avoided crossing.

O'Hare & Wahl (1972) give an equilibrium dipole moment for the $X\,^2\Pi$ state of 8.71 D, which was adopted by the JPL Molecular Spectroscopy Database (Pickett et al. 1998) to provide transition intensities. Our *ab initio* equilibrium value is $|d_{XX}(r_e)| = 8.43$ D, while the vibrationally averaged dipole moment extracted from the DUO the matrix element $|\langle v_X = 0|d_{XX}|v_X = 0\rangle|$ is 8.44 D, which is very similar to the equilibrium dipole moment. Our results suggest that JPL-predicted transitions are slightly (about 6 per cent) too strong.

3.3 Partition function

The temperature-dependent partition function for the NaO molecule was calculated as the sum

$$Q(T) = \sum_i g_i e^{\frac{-E_i}{k_B T}}, \quad (14)$$

where $g_i = g_{ns}(2J + 1)$ is the total degeneracy of the state, g_{ns} is the nuclear statistical weight factor, and k_B is the Boltzmann constant. As $Q(T)$ sums over J, the value of $Q(T)$ at some T depends on the value of J_{max} used in the sum. To ensure completeness of the line list, it is a requirement that, up to a given temperature, in the case of this study 2500 K, the value of $Q(2500)$ converges with J_{max}. As shown in Fig. 4, use $J_{max} = 200.5$ converges Q at =2500 K.

The JPL data base provides partition function values up to $T = 300$ K. Barklem & Collet (2016) provide numerical values for the partition functions of NaO up to 10 000 K, which we multiply by 4 to account for different treatments of the Na nuclear spin degeneracy;

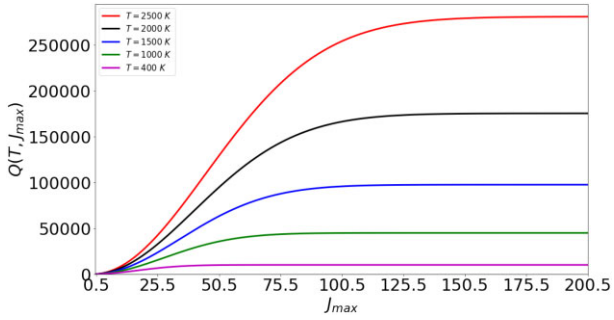

Figure 4. Partition function $Q(T)$ convergence of NaO as dependent on the maximum value of the rotational quantum number, J_{max}, for temperatures up to 2500 K.

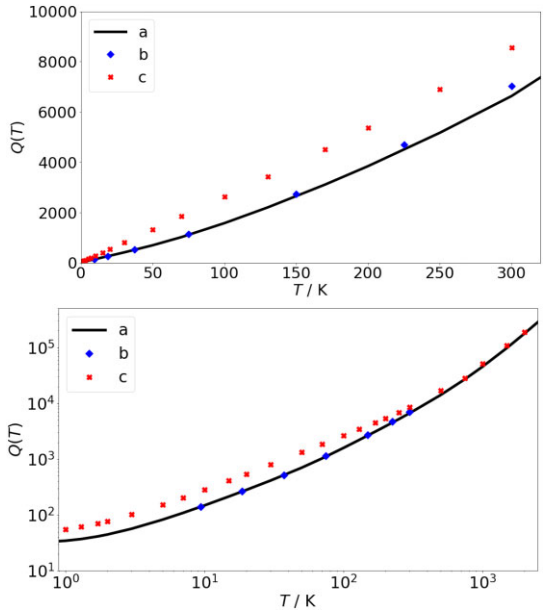

Figure 5. Comparison between the calculated partition function based on DUO states and (a) available data for the partition function of NaO, (b) Pickett et al. (1998), and (c) Barklem & Collet (2016). Note, $Q(T)$ by Barklem & Collet (2016) has been multiplied by 4 to account for the convention of including the hyperfine structure degeneration number g_{ns} in the partition function calculation, see equation (14). (Top panel) Close-up of calculated and reference partition functions for $T \in [0, 300]$ K. (Bottom panel) Log-scaled representation of calculated and reference partition functions for $T \in [0, 2500]$ K.

Table 4. Partition function, $Q(T)$, as calculated using the DUO-computed energies compared with partition functions from the JPL data base.

T (K)	Q_{DUO}	Q_{JPL}	Δ (%)
300	7027.4727	6633.1886	5.61
225	4694.9814	4491.5223	4.33
150	2734.0243	2645.0047	3.26
75	1134.4648	1109.3245	2.22
37.5	518.8865	516.1226	0.53
18.75	262.9106	262.9886	−0.030
9.375	139.2536	139.3226	−0.050

we (and JPL) include $g_{ns} = 2I_{Na} + 1 = 4$ (which is appropriate for $I_{Na} = 3/2$) in $Q(T)$, while Barklem & Collet (2016) do not. A comparison between these partition functions is given in Fig. 5. The JPL values agree well with ours (see Table 4), with the level of agreement decreasing as the temperature increases, which is probably due to the lack of the contribution of higher vibrational levels in the JPL partition sum. However, there is poor coincidence with Barklem & Collet (2016) at low temperatures, with agreement improving for higher temperature. The reason for the low-temperature disagreement between Barklem & Collet (2016) and the results of JPL and our own is unclear, but we believe that our values are correct in this region. It should be noted that the data from Barklem & Collet (2016) are based on calculated rather than experimental molecular constants taken from Huber & Herzberg (1979).

3.4 Final line list and absorption spectra simulation

The DUO package was used to produce a NaO line list, which we call NaOUCMe. This line list is given in ExoMol format (Tennyson et al. 2014, 2020) as a '∗.states' file containing term values for the lowest 36 120 rovibronic levels of the A ∼ X complex up to $J = 200.5$ and $v_X = 29$ and a '∗.trans' file consisting of the corresponding Einstein coefficients and frequencies for 4 255 242 dipole-allowed X−X, A−A and X−A transitions. In line with the updated ExoMol standard (Tennyson et al. 2020), the '∗.states' files also provide approximate uncertainties for the energies, which allow the accuracy with which we predict each transition to be estimated. For fitted regions, we recommend transition uncertainties equal to those in Table 1. For the ground electronic state, for the case where $J < 16.5$ and $v_X = 0$, an uncertainty of 0.003 cm^{-1} is recommended. Typically, energy level uncertainties scale with J quadratically, and the following functional form for $J > 15.5$ is recommended: $\delta E \approx 0.001J^2 - 0.01J + 0.01$. For all other (extrapolated) cases in the X state, the *ab initio* vibrational uncertainty takes precedence at 20–40 cm^{-1}.

The vibrational spacings between the $v_A = 0$ and $v_A = 1$ states were fitted to a satisfactory level of agreement (*artificial line* from Section 2.2). However, it is recommended that this line list only be used for high-resolution observational studies in the long-wavelength spectral range covering pure rotational transitions. Overall energy level uncertainties are summarized in Table 5.

Samples from the '∗.states' and '∗.trans' files are given in Tables 6 and 7. These were processed in ExoCross (Yurchenko, Al-Refaie & Tennyson 2018) to produce Fig. 6, an absolute absorption spectrum for the region studied by Joo et al. (1999), and Fig. 7, the absorbance cross-section for NaO as a function of temperature computed at a resolution of 1 cm^{-1} with a half-width at half-maximum (HWHM) of 1 cm^{-1}.

3.5 Comparison with the experimental X→ A spectra

The experimental A $^2\Sigma^+(0, 1) \leftarrow$ X $^2\Pi(0)$ absorption bands were observed by Joo et al. (1999) but their measurements were only sensitive in the very narrow spectral regions 2015–2095 cm^{-1} and 2646–2697 cm^{-1}. The lines in these regions were assigned to the $\Delta v = 0$ and $\Delta v = +1$ bands, respectively. An absolute intensity absorption spectrum was calculated as a stick spectrum to compare with this, see Fig. 6. The calculated absorption lines result in a line profile significantly broader than those visible from the measurements of Joo et al. (1999). The observed spectrum (relative intensities) has been scaled by matching the intensity of the strongest line [A ($J' = 7.5, v' = 0$) ← X ($J'' = 7.5, v'' = 0, \Omega'' = -1.5$)] from experiment to that of its conjugate calculated line; it can be seen that the observed $\Delta v = +1$ transitions lie on the tail-end, R-branch of the calculated absorption spectrum with a matching downward slope.

We note that Joo et al. (1999) used their measurements to determine the vibronic term value for the A(0)–X(0) band, T_0(A), namely 1992.905 cm^{-1}. Using approximate $J = 0$ zero-point energies (ZPEs) generated by DUO and $T_0(A) = T_e(A) - ZPE(X) + ZPE(A)$ shows

Table 5. Uncertainty estimates (in cm^{-1}) are applied for the rovibronic energy levels of NaO as a function of state quantum numbers.

State	X $^2\Pi$			A $^2\Sigma^+$
Case	$J_X < 16.5, v_X = 0$	$J_X > 16.5, v_X = 0$	$v_X > 0$	all v_A and J levels
Uncertainty	0.003	$0.001J_X^2 + 0.01J_X + 0.01$	20–40	10–30

Table 6. Extract from '∗.states' file produced by DUO for NaO. Lifetimes were calculated with ExoCross; for uncertainties see Section 4 and Table 5.

NN	Energy	gtot	J	Uncertainty	Lifetime	Landé	τ	e/f	State	v	Λ	Σ	Ω
1	118.305521	8	0.5	0.003000	5.1528E+03	0.001493	+	e	X2Pi	0	1	−0.5	0.5
2	704.551592	8	0.5	30.000000	2.8981E+00	0.001932	+	e	X2Pi	1	1	−0.5	0.5
3	1282.294758	8	0.5	30.000000	1.4807E+00	0.002994	+	e	X2Pi	2	1	−0.5	0.5
4	1850.69127	8	0.5	30.000000	1.0028E+00	0.012246	+	e	X2Pi	3	1	−0.5	0.5
5	2045.653545	8	0.5	20.000000	1.0894E-01	1.988261	+	e	A2Sigma	0	0	0.5	0.5
6	2409.940124	8	0.5	30.000000	6.5698E-01	0.041505	+	e	X2Pi	4	1	−0.5	0.5
7	2544.609918	8	0.5	20.000000	6.4721E-02	1.957978	+	e	A2Sigma	1	0	0.5	0.5
8	2960.425378	8	0.5	30.000000	3.7063E-01	0.112844	+	e	X2Pi	5	1	−0.5	0.5
9	3042.140902	8	0.5	20.000000	4.9272E-02	1.887345	+	e	A2Sigma	2	0	0.5	0.5
10	3501.549396	8	0.5	30.000000	1.4379E-01	0.388061	+	e	X2Pi	6	1	−0.5	0.5

Notes. NN, state counting number;
Energy, state energy in cm^{-1};
gtot, total degeneracy of the state;
J, angular momentum quantum number;
Uncertainty, energy level uncertainty in cm^{-1};
Lifetime, lifetime of the state in seconds;
Landé, Landé g factor (Semenov, Yurchenko & Tennyson 2017);
τ, parity;
e/f, rotationless parity;
State, electronic state, X2Pi or A2Sigma ;
v, vibrational quantum number;
Λ, projection of electronic angular momentum;
Σ, projection of electronic spin;
Ω, $\Lambda + \Sigma$ (projection of total electron angular momentum).

Table 7. Extract from the '∗.trans' file produced by DUO for NaO.

n_f	n_i	A_{fi}	ν_{fi}
2097	2007	7.7832E-17	0.001009
843	933	2.4392E-16	0.001035
1799	1889	9.3118E-17	0.001043
1883	1793	9.4292E-17	0.001055
1219	1309	1.6125E-16	0.001066
3848	3758	2.7618E-17	0.001137
1520	1430	1.7928E-16	0.001148
1595	1685	1.3851E-16	0.001153
3146	3056	4.9277E-17	0.001177
1688	1598	1.5019E-16	0.001179
766	676	5.6326E-16	0.001185

Notes. n_f, lower state counting number;
n_i, upper state counting number;
A_{fi}, Einstein A-coefficient in s^{-1};
ν_{fi}, transition wavenumber in cm^{-1}.

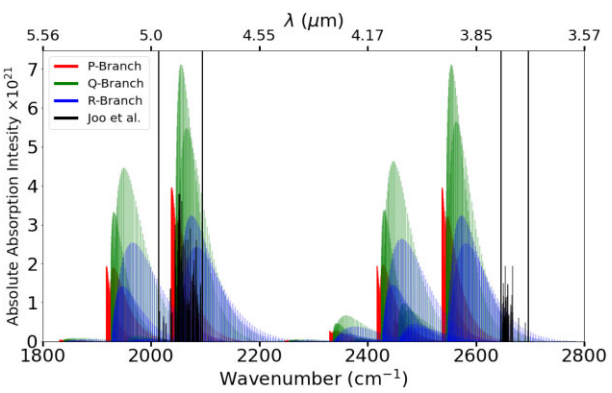

Figure 6. Absolute absorption intensity (arbitrary units) spectrum of NaO computed at $T = 400$ K. Black lines represent the experimental transitions containing (from left to right) the observed A $^2\Sigma^+(0, 1) \leftarrow$ X $^2\Pi(0)$ transition bands from Joo et al. (1999). Black vertical lines indicate the start and end of the observed band transition regions.

that our T_0(A) from our deperturbation model is 1982.3 cm^{-1}, which is less than that of Joo et al. (1999) by 10 cm^{-1}. An attempt was made to reproduce the experimental T_0(A) value above by manually adjusting T_e(A) and refitting. However, this results in significantly worse fits in the transitions (byaround an order of magnitude).

4 CONCLUSIONS

An optical line list called NaOUCMe is presented for the alkali monoxide radical, NaO, covering transitions in the 0–10000 cm^{-1} energy range up to $J = 200.5$ and $v_X = 29$ with applicability up to the equilibrium temperature $T = 2500$ K. The experimental lines for pure rotational transitions in the ground electronic state (Yamada et al. 1989) and rovibronic A $^2\Sigma^+(0, 1) \leftarrow$ X $^2\Pi(0)$ transitions (Joo et al. 1999) were used to refine the deperturbation model applied. An average rms of ∼0.006 cm^{-1} was achieved for the X $^2\Pi$ state rotational transitions and 0.35 cm^{-1} for the A $^2\Sigma^+ \leftarrow$ X $^2\Pi$ transitions, with ∼ 0.023 cm^{-1} rms for the A($v' = 0$) ← X($v'' =$

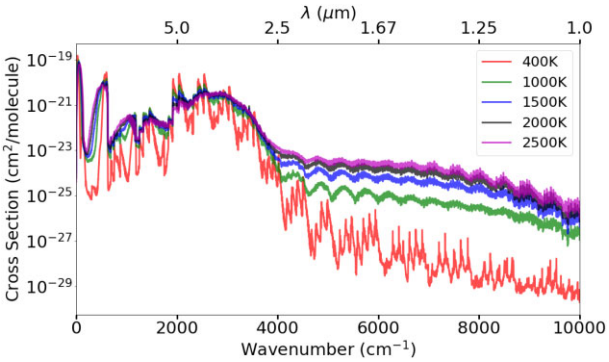

Figure 7. Spectrum of NaO at various temperatures. Absorption cross-sections were modelled with a Gaussian line profile with HWHM at 1 cm^{-1} with an output on a grid with 1 cm^{-1} spacing.

0) transitions and ~ 0.680 cm^{-1} rms for the A($v' = 1, J' = 0.5$) ← A($v'' = 0, J'' = 0.5$) *artificial line* (see Section 2.2). Uncertainties of the reproduced and predicted lines rapidly increase as the vibrational and rotational quantum numbers increase for both electronic states, and hence further experimental data on higher excited transitions are required to create a more robust line list.

The success of the CaO line list (Yurchenko et al. 2016c) in a spectrum assignment at 29 km above the Earth's surface by Berezhnoy et al. (2018) is indicative of the potential importance of s-block metal monoxides like NaO. NaO similarly is a molecule that can be studied in a terrestrial environment at approximately 90 km above the Earth's surface (Slanger et al. 2005) and has been recently studied as a transient species in air-glow by Sarkhel et al. (2009), Sarkhel et al. (2010) and Plane et al. (2012). As such, we strongly encourage further experimental study of NaO for refinement of the spectroscopic model and the production of a more accurate line list.

ACKNOWLEDGEMENTS

We thank Dr A. A. Berezhnoy for bringing the problem to our attention, and Professor I. A. Osterman for taking part in the preliminary *ab initio* calculations. This work was supported by ERC Advanced Investigator Project 883830 and by UK STFC under grant ST/R000476/1. AVS is grateful for the support by the Russian Science Foundation (RSF), grant no.18-13-00269.

DATA AVAILABILITY

The DUO model input file and calculated partition function file are given as Supporting Information to this article. The NaO NaOUCMe states and transition files can be downloaded from www.exomol.com and the CDS data centre cdsarc.u-strasbg.fr. The open access programs EXOCROSS and DUO are available from github.com/exomol.

REFERENCES

Barklem P. S., Collet R., 2016, A&A, 588, A96
Berezhnoy A. A., Borovicka J., Santos J., Rivas-Silva J. F., Sandoval L., Stolyarov A. V., Palma A., 2018, Planet Space Sci., 151, 27
Berning A., Schweizer M., Werner H.-J., Knowles P. J. P. P., 2000, Mol. Phys., 98, 1823
Boys S. F., Bernardi F., 1970, Mol. Phys., 19, 553
Buenker R. J., Liebermann H.-P., 2009, J. Chem. Phys., 131, 114107
Chapman S., 1939, ApJ, 90, 309
Huber K. P., Herzberg G., 1979, Molecular Spectra and Molecular Structure IV. Constants of Diatomic Molecules. Van Nostrand Reinhold Company, New York, NY
Joo S., Worsnop D. R., Kolb C. E., Kim S. K., Herschbach D. R., 1999, J. Phys. Chem. A, 103, 3193
Knowles P. J., Werner H.-J., 1992, Theor. Chem. Accounts, 84, 95
Kolb C. E., Elgin J. B., 1976, Nature, 263, 488
Langhoff S. R., Davidson E. R., 1974, Int. J. Quant. Chem., 8, 61
Langhoff S. R., Partridge H., Bauschlicher C. W., 1991, Chem. Phys., 153, 1
Le Roy R. J., 2017, J. Quant. Spectrosc. Radiative Transfer, 186, 179
Lee E. G., Seto J. Y., Hirao T., Bernath P. F., Le Roy R. J., 1999, J. Mol. Spectrosc., 194, 197
Lefebvre-Brion H., Field R. W., 2004, The Spectra and Dynamics of Diatomic Molecules: Revised and Enlarged Edition. Academic Press, Amsterdam
Mulliken R. S., Christy A., 1931, Phys. Rev., 38, 87
O'Hare P. A. G., Wahl A. C., 1972, J. Chem. Phys., 56, 4516
Pazyuk E., Stolyarov A., Pupyshev V., 1994, Chem. Phys. Lett., 228, 219
Pfeifer J., Gole J. L., 1984, J. Chem. Phys., 80, 565
Pickett H. M., Poynter R. L., Cohen E. A., Delitsky M. L., Pearson J. C., Müller H. S. P., 1998, J. Quant. Spectrosc. Radiative Transfer, 60, 883
Plane J. M. C., 2003, Chem. Rev., 103, 4963
Plane J., Oetjen H., Miranda M. D., Saiz-Lopez A., Gausa M., Williams B., 2012, J. Atmos. Solar-Terrestrial Phys., 74, 181
Pugh J., Shen K., Winstead C., Gole J., 1996, Chem. Phys., 202, 129
Reiher M., Wolf A., 2004, J. Chem. Phys., 121, 10945
Sarkhel S., Sekar R., Chakrabarty D., Narayanan R., 2009, Advances Earth Space Sci., 114, A10317
Sarkhel S., Sekar R., Chakrabarty D., Sridharan S., 2010, J. Geophys. Res., 115, A10306
Semenov M., Yurchenko S. N., Tennyson J., 2017, J. Mol. Spectrosc., 330, 57
Slanger T. G. et al., 2005, J. Geophys. Res., 110, D23302
Slipher V. M., 1929, PASP, 41, 262
Soldán P., Lee E. P. F., Gamblin S. D., Wright T. G., 1999, Phys. Chem. Chem. Phys., 1, 4947
Šurkus A. A., Rakauskas R. J., Bolotin A. B., 1984, Chem. Phys. Lett., 105, 291
Tennyson J., Yurchenko S. N., 2012, MNRAS, 425, 21
Tennyson J. et al., 2014, Pure Appl. Chem., 86, 1931
Tennyson J. et al., 2020, J. Quant. Spectrosc. Radiative Transfer, 255, 107228
Werner H.-J., Knowles P. J., 1985, J. Chem. Phys., 82, 5053
Werner H.-J. et al., 2010, MOLPRO, version 2010.1, a package of ab initio programs
Yamada C., Fujitake M., Hirota E., 1989, J. Chem. Phys., 90, 3033
Yurchenko S. N., Lodi L., Tennyson J., Stolyarov A. V., 2016a, Comput. Phys. Commun., 202, 262
Yurchenko S. N., Blissett A., Asari U., Vasilios M., Hill C., Tennyson J., 2016b, MNRAS, 456, 4524
Yurchenko S. N., Blissett A., Asari U., Vasilios M., Hill C., Tennyson J., 2016c, MNRAS, 456, 4524
Yurchenko S. N., Al-Refaie A. F., Tennyson J., 2018, A&A, 614, A131

SUPPORTING INFORMATION

Supplementary data are available at *MNRAS* online. Supplementary data comprise the NaO Duo input file and the partition function given in steps of 1 K.

Supplementary_Data_for_NaO.zip

Please note: Oxford University Press is not responsible for the content or functionality of any supporting materials supplied by the authors. Any queries (other than missing material) should be directed to the corresponding author for the article.

This paper has been typeset from a TEX/LATEX file prepared by the author.